Ionization via chaos assisted tunneling

Jakub Zakrzewski,[1,2] Dominique Delande,[1] and Andreas Buchleitner[3]
[1]*Laboratoire Kastler-Brossel, Tour 12, Etage 1, Universite Pierre et Marie Curie, 4 Place Jussieu, F-75005 Paris, France*
[2]*Instytut Fizyki imienia Mariana Smoluchowskiego, Uniwersytet Jagielloński, ulica Reymonta 4, PL-30-059 Kraków, Poland**
[3] *Max-Planck-Institut für Quantenoptik, Hans-Kopfermann-Strasse 1, D-85748 Garching, Federal Republic of Germany*
(Received 17 July 1997)

A simple example of quantum transport in a classically chaotic system is studied. It consists in a single state lying on a regular island (a stable primary resonance island) that may tunnel into a chaotic sea and further escape to infinity via chaotic diffusion. The specific system is realistic: It is the hydrogen atom exposed to either linearly or circularly polarized microwaves. We show that the combination of tunneling followed by chaotic diffusion leads to peculiar statistical fluctuation properties of the energy and the ionization rate, especially to enhanced fluctuations compared to the purely chaotic case. An appropriate random matrix model, whose predictions are analytically derived, describes accurately these statistical properties. [S1063-651X(98)02301-0]

PACS number(s): 05.45.+b, 32.80.Rm, 42.50.Hz

I. INTRODUCTION

Quantum systems with classically chaotic counterparts possess unique characteristic features as summarized, e.g., in [1,2]. Following the semiclassical approach, one often relates quantum properties of a system to its classical motion, using, for example, a direct comparison of phase-space portraits of the classical dynamics and wave-function quasiprobability representations in the phase space (via Husimi or Wigner functions) [1,3,4]. Even in the case of globally chaotic dynamics, individual unstable classical trajectories can be retraced by stationary quantum eigenfunctions that are ''scarred'' by the classical solution [5]. When the classical phase space is mixed (partially chaotic and partially regular), a similar separation into regular and irregular wave functions is possible in the quantum world [6]. Stable regions of phase space (tori) lend themselves to semiclassical Einstein-Brillouin-Keller quantization, yielding both the approximate eigenenergies and the corresponding wave functions [7]. Similarly, there are ''irregular'' wave functions in the region of chaotic classical motion. Some of them can be associated with residual structures of classically regular motion such as cantori while others are practically structureless. In low-dimensional systems, Kolmogorov-Arnold-Moser tori provide impenetrable borders; the only way regular and irregular wave functions may communicate with each other is by quantum-mechanical tunneling processes. In higher-dimensional systems, classical Arnold diffusion provides another mechanism of transport, a process that is, however, typically quite slow [8]. On the other hand, quantum-mechanical tunneling through impenetrable borders of classical mechanics may be quite effective. Once the particle tunnels from, say, a stable island into the surrounding chaotic phase space, it can visit distant regions following the classically chaotic transport mechanism. In particular, it can tunnel into some other stable island thus providing the coupling between two wave functions localized on distinct and separated islands or it can wander very far away (possibly leading, e.g., to ionization as in atoms driven by external radiation).

Interestingly, this ''chaos-assisted'' tunneling mechanism posseses unique features typically absent in the standard ''barrier'' tunneling of quantum mechanics, such as a great sensitivity to the variation of external parameters manifesting itself in fluctuations of observable quantities. Previous work considered mainly model one-dimensional time-dependent systems [9–11] or model two-dimensional autonomous systems [12–15]. A similar problem in the scattering case has also been discussed on a kicked model system [16]. We shall consider here a realistic, experimentally accessible (although simplified; see below) system, namely, the hydrogen atom illuminated by microwave radiation. Instead of considering tunneling between two regions (tori) mediated by the chaotic transport between them, we shall rather consider the single tunneling process out of the stable island. Then the chaotic diffusion process will lead to ionization. While in the former case the probability may flow periodically between two regions linked by the tunneling coupling, in our problem the process is irreversible and constitutes the mechanism of the decay.

The paper is organized as follows. Section II contains the description of the systems studied (the hydrogen atom in the field of a microwave radiation of either circular or linear polarization) and a general presentation of the ionization via chaos-assisted tunneling. Section III presents a simple model for the description of the fluctuations present in the decay, catalyzed by chaos-assisted tunneling. We present there the distribution of resonance widths and consider also the distribution of energy shifts of the single, initially localized state due to the coupling to other ''delocalized'' states and, via these states, to the continuum. This theory is confronted with the numerical data obtained for the hydrogen atom in the field of microwave radiation of either circular or linear polarization in Sec. IV. Finally, we present conclusions in Sec. V while the Appendix contains the details of the derivation of formulas presented in Sec. III.

*Permanent address.

II. NONDISPERSIVE ELECTRONIC WAVE PACKETS AND THEIR IONIZATION

In order to obtain the simplest study of quantum transport through a chaotic sea, one should use an initial state as localized as possible in phase space as, for example, a minimum wave packet localized on a classical stable equilibrium point. Unfortunately, in atomic systems, no stable equilibrium point of the electron outside the nucleus exists.

A simple alternative is to use a nonlinear resonance between the internal motion of the electron and an external driving force. Recently, interesting objects have been proposed in the studies of hydrogen atoms illuminated by microwave radiation of either linear [17] or circular [18] polarization: the so-called nondispersive wave packets. The corresponding classical dynamics picture corresponds to the stable resonance island embedded in a chaotic sea. For the motion contained within the principal 1:1 resonance between the Kepler frequency of the unperturbed Rydberg electron and the frequency of the driving field, the frequency of the electronic motion is locked on the external microwave frequency. Semiclassically, a wave packet localized on such a regular island will be confined to it modulo the exponentially decaying tails of the wave function that may extend into the chaotic region. In a quantum treatment, one finds wave packets that are really single eigenstates of the atom dressed by the microwave field, i.e., single eigenstates of the corresponding Floquet [19] Hamiltonian [17,20]. They are localized in all spatial dimensions and propagate along the classical trajectory in the same way a classical particle would. For a generic case (e.g., linear polarization microwaves, or, more generally, any time-periodically perturbed system [4]), it undergoes periodic deformations that faithfully follow the change of shape of the resonance island over one period, repeating the same shape every period. Only in the case of circular microwave polarization, the shape of the wave packet eigenstate does not change. This is due to the fact that the time dependence may be removed from the Hamiltonian of the problem by a transformation to the frame rotating with the field [21–23].

As mentioned above, a finite $\hbar$ value leads to quantum-mechanical tunneling from the island to the chaotic sea surrounding it. Then the electron gains energy from the driving field and eventually becomes ionized by a process classically known as chaotic diffusive ionization. Since many different paths link the initial wave packet with the continuum, its ionization time (or its reciprocal, the ionization rate or resonance width) fluctuates strongly with the parameters of the problem, the microwave frequency ω or its amplitude F [24]. Therefore, these wave packets are ideally suited for a quantitative study of the ionization promoted by chaos-assisted tunneling.

A. Circularly polarized microwave

Let us consider first the conceptually simpler case of hydrogen atoms illuminated by a circularly polarized microwave (CPM) [18,20,24]. The problem is fully three dimensional; however, as it has been shown elsewhere [20,24], one can consider the quantum dynamics in the space restricted to the polarization plane of the microwave field. While this excludes possible excitations in the direction perpendicular to the polarization plane, the dynamics of the wave packets and their properties are qualitatively not affected by the reduced dimensionality [20,24]. In the following, we shall present results obtained within such a reduced two-dimensional model.

The time dependence of the Hamiltonian describing the CPM ionization of H atoms is explicitly removed by transforming to the coordinate frame that corotates with the microwave field [21,22], where it reads (in atomic units)

$$H=\frac{\mathbf{p}^2}{2}-\frac{1}{r}+Fx-\omega\ell_z, \tag{1}$$

with ℓ_z the angular-momentum operator.

At the center of the principal resonance island between the Kepler and the microwave frequency, a periodic orbit exists whose period exactly matches the period of the microwave. In the laboratory frame, this is a circular orbit with radius x such that

$$\frac{1}{\omega^2 x^2}+\frac{F}{\omega^2}=x. \tag{2}$$

We introduce the effective principal quantum number n_0 (not necessarily an integer) corresponding to this main resonance:

$$n_0=\omega^{-1/3}. \tag{3}$$

Due to the classical scaling of the Coulomb problem [25], between the two parameters ω and F only one is necessary to tune the dynamics classically. Thus we define quantities (position and microwave electric field) scaled with respect to n_0:

$$\begin{aligned} x_0&=xn_0^{-2}=x\omega^{2/3},\\ F_0&=Fn_0^4=F\omega^{-4/3}. \end{aligned} \tag{4}$$

F_0 represents the ratio of the external microwave field to the Coulomb field of the nucleus on the unpertubed resonant circular orbit. The classical dynamics depends only on this parameter. The scaled radius x_0 of the resonant circular orbit is the solution of the scaled equation

$$\frac{1}{x_0^2}+F_0=x_0. \tag{5}$$

In the corotating frame, the resonant orbit corresponds to an equilibrium point. This point is stable if the dimensionless stability parameter

$$q=\frac{1}{\omega^2 x^3}=\frac{1}{x_0^3} \tag{6}$$

is chosen in the interval $8/9<q<1$ [18]. Then the existence of a wave packet localized in the vicinity of the fixed point is ensured in the semiclassical limit. It appears in the rotating frame as a stationary eigenstate of the Hamiltonian (1) localized around the equilibrium point and in the laboratory frame as a localized wave packet following a circular trajectory without spreading.

The energies of the wave-packet eigenstates in the rotating frame are given (in a harmonic approximation around the stable fixed point) by [20]

$$E_0=\frac{1-4q}{2q^{2/3}}\omega^{2/3}+(N_+ + \tfrac{1}{2})\omega_+ -(N_- + \tfrac{1}{2})\omega_- , \qquad (7)$$

with

$$\omega_\pm = \sqrt{\frac{2-q\pm\sqrt{q(9q-8)}}{2}}\omega \qquad (8)$$

the normal mode frequencies of the locally harmonic Hamiltonian that confines the wave packet and $N_\pm$ the number of quanta in these modes. In the following we shall consider the ionization of the ''ground-state'' wave packet corresponding to $N_+=N_-=0$. Such a wave packet can be expanded over the usual atomic eigenstates. It is a coherent superposition of mainly circular states [20]. The frequency ω is close to the resonance between atomic circular states with principal quantum numbers $n\rightarrow n\pm 1$ with $n\simeq n_0$. Thus these states are strongly coupled by the microwave field. It can be shown that, for such a frequency, the overlap of the wave packet state with circular states is, for a sufficiently high n_0, Gaussian distributed with a maximum at n_0 and the width of the order of $\sqrt{n_0}$.

To find the wave packets numerically, we diagonalize the time-independent Hamiltonian in the rotating frame (1) in a Sturmian basis [23]. The so-called complex rotation method [26] allows us to take exactly into account the coupling to the continuum. We refer the reader to Ref. [23] for a description of the technical details. Let us mention here only that a diagonalization yields complex energies $E_i-i\Gamma_i/2$, where the real parts E_i are the positions of the resonances, while the Γ_i correspond to their widths, i.e., their ionization rates. In this approach, spontaneous emission from the wave-packet eigenstates to lower-lying states is neglected. This is a reasonable approximation as they are composed of mainly circular states that have very long spontaneous lifetimes, typically of the order of several 10^6 periods. In all calculations discussed hereafter, the decay of wave-packet eigenstates is dominated by field-induced ionization (via chaos-assisted tunneling) and *not* by spontaneous emission [27,28].

The present results are obtained from the diagonalization of matrices of size up to 200 000. We use the Lanczos algorithm [29] to extract few eigenvalues and the corresponding eigenvectors in the vicinity of the energy predicted by the semiclassical expression (7). The wave-packet eigenstate is then identified by its large overlap with the circular state with principal quantum number close to $n_0=\omega^{-1/3}$ and by its large dipole moment. Typically, due to the accuracy of the semiclassical prediction, it is enough to extract a few eigenvalues of the matrix. For our present purpose, it is the *deviation* of the exact resonance position from the semiclassical prediction and the *ionization rate* that are of great interest for us.

For our statistical analysis, it is reasonable to collect the data for a *fixed* classical dynamics, i.e., at *fixed* F_0 value varying simultaneously ω and F around some mean values. On the other hand, quantum mechanics does *not* preserve the classical scaling: The finite $\hbar$ value introduces another scale into the problem, say, the energy of the state or the number of photons necessary for the ionization. We shall see that this has important consequences for the characteristics of the ionization process: The statistical properties of the widths depend on n_0.

We shall present the numerical data for both circular and linear polarization of the driving field simultaneously. Thus, before presenting the data, we review the wave-packet properties in a linearly polarized microwave (LPM) [17].

B. Linearly polarized microwave

If the atom is irradiated by an electromagnetic field of linear polarization defining the z axis, the angular-momentum projection m on the field axis is a good quantum number, due to the rotational symmetry of the Hamiltonian

$$H=\frac{\mathbf{p}^2}{2}-\frac{1}{r}+Fz\,\cos(\omega t). \qquad (9)$$

One is therefore left with two spatial degrees of freedom and the explicit, time periodic dependence of the Hamiltonian that cannot be eliminated. However, the temporal periocicity of the problem (for constant driving field amplitude F) allows for the application of the Floquet theorem and the identification of the eigenfunctions $|\psi_i\rangle$ of the atom *in* the field as solutions of the stationary Floquet equation [19]

$$(H-i\partial_t)|\psi_i\rangle=E_i|\psi_i\rangle, \qquad (10)$$

where spatial coordinates and time are treated now on an equal footing. The Floquet theorem guarantees that the eigenfunctions $|\psi_i\rangle$ are periodic with the period $T=2\pi/\omega$ of the driving field and form a complete basis of the problem. The Floquet states with quasienergies E_i are nothing but the ''dressed states'' of the atom in the field [30].

Again, when Coulomb attraction and driving field amplitude become comparable, the classical dynamics of the Rydberg electron turns chaotic and phase space is divided into regions of regular and irregular motion. At sufficiently large field amplitudes, only the principal resonance between the driving frequency and the Kepler motion is left as an (elliptic) island of regular motion in the chaotic sea [17]. Unlike the circularly polarized microwave (CPM) case, the stable periodic orbit at the center of the elliptic island is not characterized by a set of simple analytical expressions. However, the local oscillatory motion can be plugged into the form of a Mathieu equation [31], the numerical solution of which provides good estimates of the energy of the quantum-mechanical ground state and of the first excited states of the local Hamiltonian [4,32]. The oscillator ground state is the wave-packet eigenstate of the atom in the field and follows the classical, periodic evolution of the principal resonance island [17,33]. Depending on the value of the classical angular momentum and its projection on the symmetry axis, the wave packet may probe the Coulomb singularity and consequently displays some transient dispersion that mimics the acceleration of the classical particle at the aphelion [17].

Since, in the LPM case, the numerical detection of the wave packet is less straightforward than for CPMs, we restrict ourselves to the investigation of the hydrogen atom

confined to one spatial dimension, along the field polarization axis. As the driving field amplitude is increased, it is this direction along which chaos is born in the full dynamics of the three-dimensional atom [17,34,35], and therefore this approximation will be sufficient for our present purposes.

The LPM case has the same scaling property as the CPM case: The classical dynamics depends only on the scaled field $F_0 = F\omega^{-4/3}$. Numerically, the wave packets are identified by their large (compared to other nearby Floquet states) overlap with the state $|n_0\rangle$ [36], which is resonantly coupled to its nearest neighbor $|n_0+1\rangle$ by the driving frequency. Similarly to the CPM case, the quasienergies E_i and resonance widths Γ_i of the wave packets are used for the statistical analysis. All data samples are characterized by a fixed value of the parameter F_0, hence they correspond to the same structure of classical phase space. For a given value of F_0, ω (and, accordingly, F) has been scanned to give 1000 eigenvalues per F_0 value.

C. Numerical results

The typical behavior of the wave packet ionization width versus the microwave frequency has already been presented in [24] for a fixed microwave amplitude. It displays very strong fluctuations over several orders of magnitude for small changes of the frequency (typically of the order of 1 part in 1000). These fluctuations, although perfectly deterministic, look completely random and are strongly reminiscent of the universal conductance fluctuations observed in mesoscopic systems [37]. Indeed, the ionization width measures the rate at which an electron initially localized close to the stable resonant trajectory ionizes, i.e., escapes to infinity. In other words, the ionization width directly measures the conductance of the atomic system from the initial point to infinity. In the quantum language, the ionization width is due to the coupling (via tunnel effect) between the localized wave packet and states lying in the chaotic sea surrounding it. While the energy (or quasienergy in the LPM case) of the wave packet is a smooth function of the parameters F and ω, [see Eq. (7)], the energies of the chaotic states display a complicated behavior characterized by level repulsion and strong avoided crossings. By chance, it may happen that, for specific values of the parameters, there is a quasidegeneracy between the wave-packet eigenstate and a chaotic state. There the two states are more efficiently coupled by tunneling and the ionization width of the wave-packet eigenstate increases. This is the very origin of the observed fluctuations. Simultaneously, the repulsion between the two states should slightly modify the energy (real part of the complex eigenvalue) of the wave-packet state. A simple way of measuring this effect is to compute also the shift of the real part of the energy level with respect to its semiclassical position (which does not exhibit the repulsion from a near-degenerate state).

As mentioned above, we study the fluctuations for a fixed value of the classically scaling parameter F_0 versus $n_0 = \omega^{-1/3}$. Exemplary ionization width and *level shift* fluctuations are presented in Fig. 1 on a logarithmic scale for the CPM case. Note that both quantities fluctuate over several orders of magnitude and that the widths are more sensitive to changes of n_0. Since the shifts can take both positive and negative values, the absolute value of shifts is plotted.

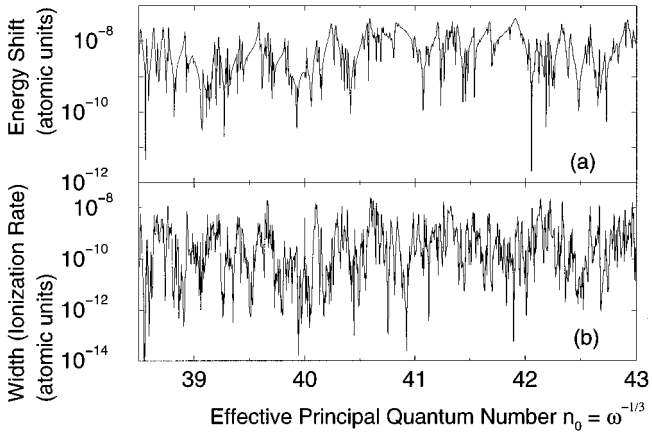

FIG. 1. Typical fluctuations of the width (ionization rate) and the energy shift (with respect to its unperturbed position) of the nonspreading wave packet of a hydrogen atom exposed to a circularly polarized microwave field. The wave packet is a stationary state of the atom dressed by the microwave field and at the same time a wave packet orbiting around the nucleus at exactly the microwave frequency, without spreading. In the language of nonlinear physics, the wave packet is at the center of the primary resonance island between the microwave frequency and the internal Kepler frequency of the electron. It is coupled to the surrounding chaotic states by tunneling and therefore has an ionization rate induced by a chaos-assisted tunneling process that shows huge fluctuations when a parameter is varied. The data presented are obtained for small variations of the effective principal quantum number n_0 around 40, a scaled microwave electric field $F_0 = Fn_0^4 = 0.0426$, and a microwave frequency $\omega = 1/n_0^3$. To present both plots on a logarithmic scale (more convenient to show the fluctuations over several orders of magnitude) we plot the absolute value of the shift rather than the shift itself.

Importantly we must mention that the shifts plotted in Fig. 1 and used later for the statistical analysis are not obtained directly from the difference between the resonance energy and the semiclassical prediction (7) as anticipated before. These differences show a bias: The average shift is nonzero. It indicates that although Eq. (7) well predicts the wave-packet energy (to within a fraction of the mean level spacing), the remaining difference is not solely due to the fluctuations. There is a slowly varying part in it that most probably originates from the unharmonic corrections. The latter could be estimated; however, since in the LPM case we do not have any good semiclassical prediction, we find the fluctuating part of the shift in both cases by subtracting from the exact quantum energies the smooth background. The latter is obtained by a low-order polynomial fit of the wave-packet eigenenergies as a function of the parameter n_0.

To describe the fluctuations *quantitatively*, which is the main aim of this study, we calculate the statistical distributions of the ionization widths $P(w)$ and of the energy shifts $P(s)$. Typical distributions are displayed as histograms on a double-logarithmic scale in Fig. 2. The data are those of Fig. 1. The use of logarithmic scales is useful to show quantitatively the fluctuations over several orders of magnitudes. From this figure, we immediately obtain the following qualitative conclusions.

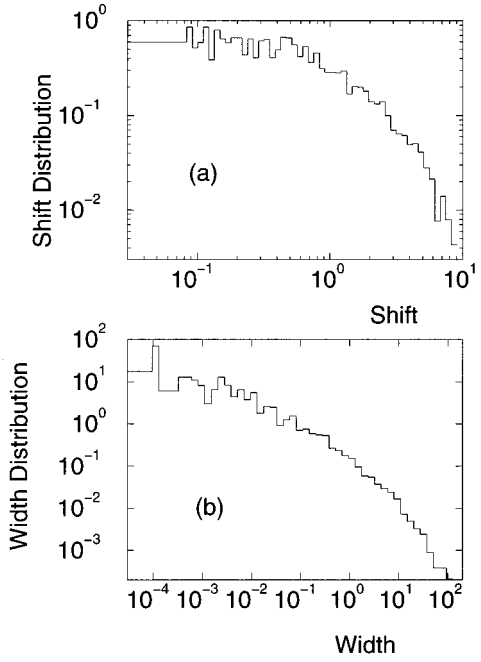

FIG. 2. Distributions of the (a) energy shifts and (b) widths of the nonspreading wave packet of a hydrogen atom in a circularly polarized microwave field. The data are those of Fig. 1. They are plotted on a double-logarithmic scale, which clearly shows the large fluctuations. Both the shift (actually the absolute value of the shift) and the width have been rescaled to their typical values, as explained in the text.

(i) The distribution of energy shifts $P(s)$ tends to a constant as $s \to 0$.

(ii) Above some critical value, the distribution drops and decreases roughly algebraically with s. The slope is close to -2, indicating a $P(s) \equiv 1/s^2$ behavior.

(iii) Finally, $P(s)$ falls off abruptly above some value.

(iv) The distribution of ionization widths $P(w)$ behaves algebraically with w at small width, with a slope close to $-1/2$. Hence the small widths are the most probable ones.

(v) Above some critical value, the distribution drops faster, roughly with a $1/w^{3/2}$ behavior.

(vi) Finally, similarly to the shift distribution, there is a final sharp cutoff.

These conclusions are similar to the ones obtained in a slightly different physical situation, when two symmetric regular islands are coupled to a single chaotic sea (see Ref. [14] for a complete discussion of this physical situation). There, states lying on the regular islands appear in doublets with even or odd parities with respect to the discrete symmetry exchanging the two regular islands. The splitting of the doublet is a direct measure of the chaos-assisted process where the particle tunnels from one regular island, then diffuses in the chaotic sea, and finally tunnels to the other regular island. This process is very similar to the one studied in the present paper where the particle tunnels and then diffuses towards infinity. The splitting distribution observed in [14,15] is indeed very similar to our shift distribution as explained below. In the following section, we propose a simple model, mainly based on physical ideas similar to those used in [14], that allows us to understand the properties of our shift and width distributions.

III. STATISTICAL MODEL

We shall consider a simple statistical model amenable to an analytical treatment. Despite its simplicity, we shall see 'that it is capable of describing quantitatively the fluctuations of resonance widths and shifts observed in the numerical analysis of the microwave ionization of hydrogen atoms.

The model system is directly based on the understanding we have of the origin of the fluctuations and follows the idea already used in [14]. The idea is to consider the wave-packet eigenstate as coupled randomly to a set of chaotic states (described by random matrix theory), which are themselves randomly coupled to the atomic continuum. More precisely, our model consists of a single state $|0\rangle$ (representing a state localized on the elliptic island) coupled (weakly) to the space of N ''chaotic,'' irregular levels, which are close to $|0\rangle$ in energy. The latter states are considered to be, strictly speaking, resonances rather than bound states due to the mechanism responsible for decay (e.g., the ionization of an atom). While we consider a single localized state in the model, there may be several other states localized on the same island. They will have typically much different energies and their mutual coupling via the chaotic states is negligible.

The Hamiltonian matrix may be represented as an $(N+1)\times(N+1)$ matrix:

$$\mathcal{H} = \begin{pmatrix} 0 & \sigma\langle V| \\ \sigma|V\rangle & H_0 - i\mathcal{W} \end{pmatrix}, \tag{11}$$

where we have assumed that the energy of the localized state sets the zero of the energy scale. The first vector in the basis represents the localized state, the following N ones the chaotic states. In the chaotic subspace, the statistical properties of the Hamiltonian are well represented by an $N \times N$ random matrix H_0. We shall deal with problems with a preserved (generalized) time-reversal invariance: H_0 should belong, therefore, to the Gaussian orthogonal ensemble (GOE) of real symmetric matrices [2,38]. The matrix elements of H_0 are independent random Gaussian variables

$$P((H_0)_{ij}) = \frac{\exp\left(-\dfrac{(H_0)_{ij}^2}{2\sigma_{ij}^2}\right)}{\sqrt{2\pi\sigma_{ij}^2}}, \tag{12}$$

with the variance satisfying

$$\sigma_{ij}^2 = (1+\delta_{ij})\frac{\pi^2\Delta^2}{N}. \tag{13}$$

Here Δ is the mean level spacing between consecutive chaotic states close to energy 0.

Following a commonly accepted approach [39], the coupling of the chaotic state to the continuum is introduced by the decay matrix

$$\mathcal{W} = \frac{\gamma}{2}|W\rangle\langle W|, \tag{14}$$

where the N component real vector $|W\rangle$ describes the coupling of the chaotic states to the continuum. As in Ref. [39], we take this vector to be composed of Gaussian distributed random numbers with vanishing mean and unit variance. The real coefficient γ measures the strength of the decay to the continuum. Such a form implies that there is only one significant decay channel for chaotic states. This is far from obvious and, as discussed below, probably true only at relatively low field strength. When there are several open ionization channels, a convenient form of the decay matrix is [39]

$$\mathcal{W}=\sum_{k=1}^{M}\frac{\gamma_k}{2}|W^{[k]}\rangle\langle W^{[k]}|, \tag{15}$$

where M denotes the number of open channels (degeneracy of the continuum) and the N component real vectors $|W^{[k]}\rangle$ describe the coupling of the chaotic states to channels $k=1,\ldots,M$. Again, we take these vectors to be composed of Gaussian distributed random numbers with vanishing mean and unit variance. The γ_k real coefficients measure the strength of the decay to continuum k.

In a similar way, the (real) N-component vector $|V\rangle$ in Eq. (11) describes the coupling of the localized state $|0\rangle$ to the chaotic states. Each component of $|V\rangle$ is taken as a Gaussian distributed random number of zero mean and unit variance. The coefficient σ in Eq. (11) is a measure of the strength of the coupling between the localized state and the chaotic subspace.

If the coupling to the continuum is neglected ($\gamma=0$), the model describes a single bound state randomly coupled to N chaotic states. This is exactly the model succesfully used in [14] to describe the splitting of doublets induced by chaos-assisted tunneling.

The model has several free parameters: the mean level spacing between chaotic states Δ, the strength of the coupling with the ionization channel γ, and the strength of the coupling to the localized state σ. There is a trivial scaling law of the Hamiltonian $\mathcal{H}$ [Eq. (11)], which implies that, except for a global multiplicative factor, there are only two relevant dimensionless parameters σ/Δ and γ/Δ in the model. For several open channels, the relevant parameters are σ/Δ and γ_k/Δ, $k=1,\ldots,M$.

Due to the interaction with chaotic resonances, the state $|0\rangle$ is not an eigenstate of the full Hamiltonian $\mathcal{H}$ [Eq. (11)]. However, in most cases, the coupling to chaotic resonances is weak and the true eigenstate does not differ very much from $|0\rangle$: This is the perturbative regime that we shall consider in the rest of this paper. This regime is obtained when the coupling is much smaller than the mean level spacing between chaotic states, i.e.,

$$\sigma\ll\Delta. \tag{16}$$

We will see below that this condition is always satisfied for the real physical system (hydrogen atom plus microwave field) for the microwave fields studied in this paper. At very high field, when the nondispersive wave packet is destroyed, this pertubative approximation should break down. The physical interpretation is clear: If Eq. (16) is not satisfied, the localized state is spread over several eigenstates of $\mathcal{H}$ and completely loses its identity. It has been shown elsewhere [40] that, in the perturbative regime, the localized state can be interpreted as a soliton weakly interacting with the background of chaotic states, but essentially keeping its shape when a parameter (for example, the microwave field strength) is varied.

In the following, we will also assume that the ionization rates (widths) of the chaotic states are small compared to their mean level spacing, i.e., that the decay matrix W [Eq. (15)] can be considered as a pertubation. This implies

$$\gamma\ll\Delta. \tag{17}$$

Such a condition is not *strictly* necessary, but it makes calculations simpler. Physically, it means that the various chaotic resonances are isolated. This is a typical situation in our system: the ionization of an atom in the presence of microwave driving for not too strong microwave amplitudes.

With the above assumptions, motivated by the physics of the process studied, the shift and width of the localized state may be obtained using the lowest nonvanishing order of perturbation theory. Such an approach is justified unless an accidental degeneracy between the localized state and one of the eigenstates of the matrix H_0 occurs. Neglecting such degeneracies (which only affect the tail of the distribution; see Sec. IV A below) and performing an average over the random matrix ensemble defined by Eq. (11) makes it possible to extract the analytic expressions both for the distribution of shifts and for the distribution of widths. The details of the derivation are given in the Appendix. We give here only the important results.

The shift distribution is obtained along a similar way to Leyvraz and Ullmo [15] and takes the form of a Cauchy law

$$P(s)=\frac{1}{\pi}\frac{s_0}{s_0^2+s^2}, \tag{18}$$

with

$$s_0=\frac{\pi\sigma^2}{\Delta}. \tag{19}$$

Importantly, this result is independent of the degree of correlation among the eigenvalues of the H_0 matrix: The same result is obtained for an uncorrelated spectrum (Poisson-like distributed eigenvalues, physically corresponding to coupling of the localized state with a set of ''regular'' states, instead of chaotic ones as in the model described above), a GOE, or a picket-fence (harmonic-ocsillator) spectrum [15]. This Cauchy distribution is the same as the one obtained [14,15] in the absence of ionization.

The situation is a bit more complicated for the width distribution. For Poissonian distributed eigenvalues of H_0 (uncorrelated spectrum), a similar Cauchy distribution is obtained for the *square root* of the width, corresponding to the following distribution of widths (see the Appendix):

$$P_{\mathrm{Poisson}}(w)=\frac{1}{\pi}\frac{\sqrt{w_0}}{\sqrt{w}(w+w_0)}, \tag{20}$$

with

$$w_0 = \frac{4\sigma^2\gamma}{\Delta^2}. \tag{21}$$

For a matrix H_0 belonging to the GOE, the distribution is slightly more complicated (see the Appendix):

$$P_{\mathrm{GOE}}(w) = \frac{2}{\pi^2}\frac{w_0'^{3/2}\ln(w+\sqrt{1+w/w_0'})+\sqrt{ww_0'(w+w_0')}}{w(w+w_0')^{3/2}}, \tag{22}$$

with

$$w_0' = \frac{\pi^2\sigma^2\gamma}{\Delta^2} = \frac{\pi^2}{4}w_0. \tag{23}$$

Although it is distinct from Eq. (20), it has in fact quite a similar shape (see Fig. 4). In particular, if P_{GOE} is rescaled by a global multiplicative factor of about 20%, it is almost indistinguishable from P_{Poisson}. Many statistics are necessary to determine which of the two distributions is the correct one for a given data set (see also Sec. IV).

We can also obtain the distribution of widths for the chaotic states in the perturbative regime. This is the well-known ''nonoverlaping resonances'' regime [41–43] where the widths are distributed according to a Porter-Thomas distribution

$$P_{\mathrm{PT}}(w) = \frac{1}{\sqrt{w\overline{w}}}\exp(-w/2\overline{w}), \tag{24}$$

where $\overline{w}$ denotes the average width. For small w, P_{PT} diverges as $w^{-1/2}$, while for large w it decays exponentially.

IV. ANALYSIS OF THE DATA

A. Quantitative analysis of the fluctuations with the statistical model

The exact expressions (18–22), obtained in the perturbative regime reproduce qualitatively most of the statistical distributions numerically observed for the shift and width of the nondispersive wave packet of the hydrogen atom in a microwave field; see Fig. 2. For the shift distribution $P(s)$, the distribution is constant near 0 and decays like $1/s^2$ at large s. The only difference is the absence of the sharp cutoff in the perturbative expression. This can be easily understood: The large energy shifts correspond to quasidegeneracies between the localized state and one specific chaotic state, i.e., to the immediate vicinity of an avoided crossing. There the simple pertubative scheme breaks down and the actual shift remains finite as the perturbative expression diverges as the inverse of the unperturbed spacing between the chaotic and localized states. Hence the actual distribution has to fall faster than the perturbative one at large shifts, as numerically observed.

The width (ionization rate) distribution behaves similarly. Both the initial $1/w^{1/2}$ regime and the following $1/w^{3/2}$ regime observed for the wave packet are well reproduced by the simple statistical model. Again, the difference is the absence of the cutoff for very large widths. The reason is identical, namely, the breakdown of the perturbative approximation.

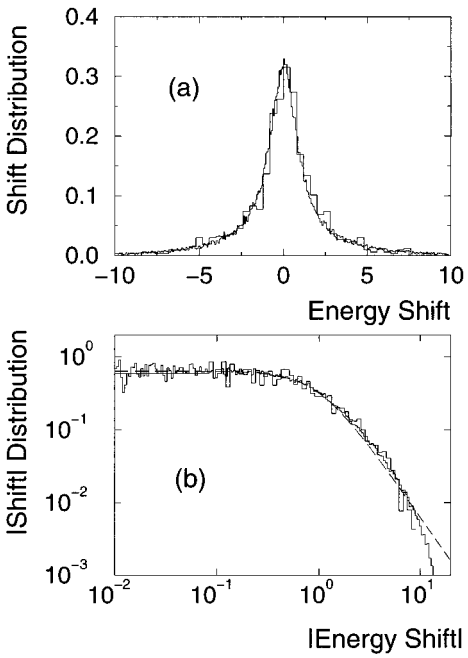

FIG. 3. Comparison between the distributions of the energy shifts of the nonspreading wave packet of a hydrogen atom in a circularly polarized microwave (large bins histogram) with the distribution obtained for our random matrix model (small bins histogram). The data are those of Fig. 1 with the same rescaling. (a) Linear scale; the agreement is excellent. The two histograms follow exactly a Cauchy distribution (18). (b) Double-logarithmic scale, which emphasizes the long tail of the distributions. Again, the agreement is remarkable. The dashed line is the pure Cauchy distribution predicted in the perturbative regime and differs from the numerical result at large shifts.

Nevertheless, we can go beyond the perturbative scheme, using the statistical model described in Sec. III, but calculating numerically the shift and width distribution. This has been done by numerical diagonalization of the complex Hamiltonian, i.e., of random matrices corresponding to Eq. (11), generated according to the rules given above. A diagonalization of a matrix of size $N=80$ yields a single shift and width for chosen values of σ/Δ and γ/Δ. Using different random matrix realizations we accumulate up to 50 000 data for comparison. We have verified that the distributions obtained do not depend on the matrix size N.

In Fig. 3 we show the numerical results for the shift distribution obtained for the hydrogen atom in a circularly polarized microwave field with the perturbative analytical expression for our random matrix model (pure Cauchy distribution) [Eq. (18)] and with the full nonperturbative result using our statistical model, both on a linear scale, well suited for small and moderate shifts, and on a double logarithmic scale, well suited for the tail of the distribution at large shifts. As expected, the perturbative analytical expression reproduces the numerically observed distribution, except for the exponentially small tail at a large shift. The full nonperturbative distribution is found to be in excellent agreement with the numerical data for the real system, the hydro-

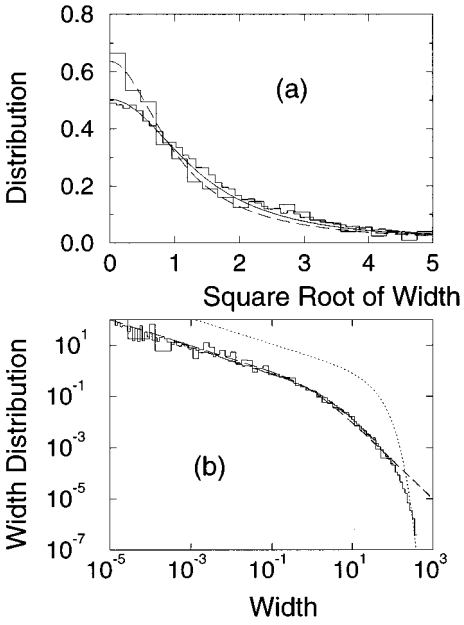

FIG. 4. Same as Fig. 3, but for the width. (a) Linear scale for the distribution of the square root of the width. The dashed line is the analytical result (Cauchy distribution), Eq. (20), for a Poisson spectrum and the continuous solid line the analytical result (22) for a GOE spectrum. The agreement with the Poisson prediction is slightly better, although all distributions are very similar. (b) Double-logarithmic scale showing the agreement of the random matrix model with the real system, even for the tail of the distribution. The dashed line is the analytical perturbative expression (20), which differs from the numerical result in the tail. The dotted line is the Porter-Thomas distribution (24) for a system without chaos-assisted tunneling; it describes the exponentially small tail of the distribution.

gen atom in a circularly polarized microwave field, which proves that our simple statistical model actually catches the physics of the chaos-assisted tunneling phenomenon. A similar conclusion has been reached [14] for doublet splittings induced by chaos-assisted tunneling.

In Fig. 4 a similar analysis is done for the distribution of widths, on both a linear and a double-logarithmic scale. On the linear scale, instead of the width distribution (22) itself, which diverges at zero (see the Appendix), we plotted the distribution for the square root of the width, which tends to a constant value at zero. As can be seen, the agreement is again excellent over the full range, the perturbative expression being inaccurate in the tail only, as expected. In addition to the perturbative analytical expression (22) we have also drawn the distribution expected when the states in the chaotic sea have eigenergies described by a Poisson distribution rather than a GOE one (20). Both distributions are similar far from the origin and differ by about 20% at $w=0$. At first glance, it seems that the Poisson curve agrees slightly better than the GOE curve, which is somewhat surprising and not understood as chaotic motion surrounding the stable island suggests the choice of the GOE. However, the deviation is at the border of statistical significance. In the double-logarithmic plot, we have also added the Porter-Thomas distribution (24), which reproduces correctly the tail at large widths.

It is remarkable that both the shift and the width distributions are so well reproduced by the random matrix model. This proves that our simple statistical model carries the essential part of the physics. The data presented are the first, as far as we know, manifestation of the chaos-assisted tunneling process in a realistic, experimentally accessible systems.

Even if the perturbative expression (20) incorrectly describes the nonperturbative large width tail, it is clear that the initial $w^{-1/2}$ decrease, similar to P_{PT} [Eq. (24)] is followed by a regime of $w^{-3/2}$ behavior. The length of this $w^{-3/2}$ behavior provides interesting information about the system. For strong coupling, $\sigma \geqslant \Delta$, the localized state $|0\rangle$ is strongly mixed with the chaotic state. Thus its width distribution would be the same as that of other resonance states, i.e., a Porter-Thomas distribution. Hence the $w^{-3/2}$ part there shrinks to zero and the power $-1/2$ law is followed immediately by the exponential tail. The relative importance of the $w^{-3/2}$ part in the width distribution indicates, therefore, the presence of the weak-coupling, perturbative regime. Compared to the pure chaotic state where fluctuations of the widths are already known to be large, the effect of additional tunneling is to shift some part of the width distribution towards small widths while keeping the exponential cutoff, that is, to increase the fluctuations. In the perturbative limit, the fluctuations become so large that the average width *diverges*.

The success of the statistical model allows to give a complete physical interpretation of the observed data.

(i) The smallest shifts and widths, observed for

$$s < s_0, \tag{25}$$

$$w < w_0, \tag{26}$$

with probabilities behaving, respectively, as s^0 and $w^{-1/2}$, correspond to the localized state lying far from quasidegeneracies with one of the chaotic states. Then the localized state is weakly contaminated by the various surrouding chaotic levels. For example, its shift is the sum of the effect of level repulsion by the various chaotic states. Chaotic states with higher (lower) energy push the localized state down (up) in energy, which globally results in a small shift with a random sign. The width results from the interference between the elementary ionization amplitudes contributed by the various chaotic states. As there is only one open decay channel, the amplitudes, not the probabilities, have to be added. As they are essentially random uncorrelated variables, the interference is mainly destructive, producing small widths with a large probability.

(ii) The intermediate shifts and widths, observed for

$$s_0 < s \ll \sigma, \tag{27}$$

$$w_0 < w \ll \gamma, \tag{28}$$

with probabilities behaving, respectively, as s^{-2} and $w^{-3/2}$, correspond to one chaotic state being much closer in energy to the localized state than to the other chaotic states, but nevertheless sufficiently far to be coupled only perturbatively. Then the single coupling to this particular chaotic state dominates both the shift and the width of the localized state.

(iii) The largest shifts and widths, observed for

$$s \simeq \sigma, \tag{29}$$

$$w \simeq \gamma, \tag{30}$$

correspond to the quasidegeneracy between the localized state and one chaotic state, with strong nonperturbative mixing between the two. This is where the exponentially decreasing tails are observed.

In the latter two cases, as one chaotic state is dominant, approximate expressions for the distributions can be obtained by a simple two-level model. Although the expression of the shift and the width are then easy to obtain (diagonalization of a 2×2 complex matrix), we have not been able to perform analytically the averaging over the ensemble of random matrices.

B. Extraction of the relevant physical parameters from the statistical data

The simplest possible measures of the fluctuations of a quantity are typically its average value and the variance. Inspection of the perturbative distributions for both the shifts [Eq. (18)] and the widths [Eq. (20)] suggests, however, some caution. Indeed, the average value of the width is not defined (the corresponding integral diverges) and the same is true for the variance of the shift (the average value is zero due to the symmetry of the distribution). This is because of the existence of long algebraic tails $1/s^2$ and $1/w^{3/2}$ in the distributions. The variance of the shift and the average value of the width are infinite because of the diverging contributions of these tails. This is an example of unusual random processes such as Lévy flights [44], where rare events play the dominant role. Ultimately, it is because, in perturbation theory, the contamination of a state by its neighbors is proportional to the ratio of the coupling matrix element to the energy difference and consequently decreases slowly: Even a far distant level can have a large effect.

For the full nonperturbative distributions, the exponential cutoff at large values destroys the divergence of the various integrals, and average values and variances, as well as higher moments of the distributions, are well defined and could be calculated. Their precise values, however, depend crucially on the position of the cutoffs. Hence distributions identical for small widths (shifts) and only differing at large widths (shifts) may have completely different average values and variances. Calculating such quantities requires a very accurate knowledge of the tails of the distributions. The average values and the variances are thus fragile and difficult to calculate on a real system such as the hydrogen atom in a microwave field; they do not provide us with the most interesting physical information.

Rather than the average values, we prefer to define typical values. The typical width $\tilde{w}$ lies at the middle of the distribution, such that half of the widths are larger and half of them smaller, i.e.,

$$\int_0^{\tilde{w}} P(w)dw = \frac{1}{2}. \tag{31}$$

With such a definition, the typical width is robust, only weakly sensitive to the tail of the distribution.

A similar definition holds for the typical shift, slightly modified to take into account that s can be either positive or negative:

$$\int_0^{\tilde{s}} P(|s|)d|s| = \frac{1}{2}. \tag{32}$$

For the perturbative distributions in the statistical random matrix model, the typical widths and shifts can be calculated from Eqs. (18), (20), and (22):

$$\tilde{s} = \frac{\pi\sigma^2}{\Delta},$$

$$\tilde{w} = \frac{4\sigma^2\gamma}{\Delta^2} \quad \text{for a Poisson spectrum,} \tag{33}$$

$$\tilde{w} = \frac{5.48\sigma^2\gamma}{\Delta^2} \quad \text{for a GOE spectrum.}$$

For the full non-perturbative random model distributions, as long as the basic hypotheses of small coupling [Eqs. (16) and (17)] are true, we carefully checked that the typical widths and shifts are not significantly (within 10 or 20 %) different from the previous analytic expressions.

For a real physical system such as the wave packets in the hydrogen atom exposed to a microwave field, we can reliably extract from the statistical data the typical width and shift. We have also compared the numerically obtained distributions with nonperturbative distributions of our statistical model and performed best fits of the former by the latter. Again, we checked that the typical width and shift for the best fit do not differ by more than 10 or 20 % from the direct measures. This implies that the typical shift and width can be safely used to extract from the statistical distributions the relevant physical parameters σ (coupling between the localized state and the chaotic states) and γ (ionization widths of the chaotic states). Slightly different values are obtained if the Poisson or GOE expressions are used. In the following, we have used the GOE expression.

In fact, only σ^2/Δ and the dimensionless parameter γ/Δ (from the ratio $\tilde{w}/\tilde{s}$) can be easily extracted. Obtaining the other dimensionless parameter σ/Δ or σ and γ themselves requires knowledge of the mean spacing Δ between chaotic resonances. Surprisingly, this is not straightforward. To understand the problem, consider the diagonalization of the Floquet Hamiltonian for the LPM case. The number of states present in a single Floquet zone depends on the number of photon blocks included in the diagonalization. When it is increased, new states appear in the vicinity of the wave packet state corresponding to either low-lying atomic states (with very different energy but shifted upward by an integer times the photon frequency) or highly excited states or resonances (shifted downward). These states should not contribute to the determination of Δ since they have a vanishing overlap with atomic states building the wave packet. Hence the mean level spacing Δ between chaotic states is a somewhat ambiguous quantity. However, as will be seen at the

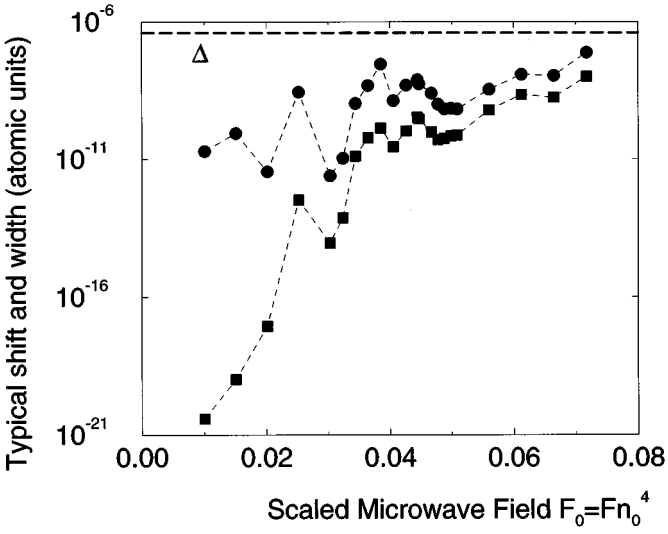

FIG. 5. Typical shift (with respect to the unperturbed energy level) and width (ionization rate) of the nonspreading wave packet of the hydrogen atom in a circularly polarized microwave. Each point in the plot is extracted from the analysis of a distribution similar to the one in Fig. 2 built from several hundred independent diagonalizations of the Hamiltonian (1) at neighboring values of the field strength and frequency, around $n_0=40$. The statistical analysis of each distribution is done as in Figs. 3 and 4. The typical values of the energy shift (circles) and width (squares) globally increase with the microwave field strength, but with bumps that are obviously correlated. The long-dashed line represents the mean energy level spacing Δ between chaotic levels (all quantities are plotted in atomic units). The typical width is smaller than the typical shift, itself smaller than Δ, which proves that the data are obtained in the perturbative regime where chaos-assisted tunneling is only a small perturbation. For details, see the text.

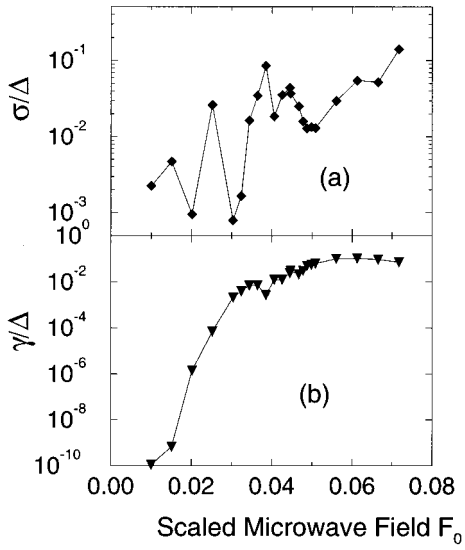

FIG. 6. Nonspreading wave packet of a hydrogen atom in a circularly polarized microwave. The tunneling rate to the (a) surrounding chaotic sea σ/Δ and (b) chaotic ionization rate γ/Δ of the chaotic states is as extracted from the data in Fig. 5, using our simple statistical model based on random matrix theory. These two quantities are dimensionless (rescaled to the mean level spacing) and smaller than 1 in the perturbative regime. The tunneling rate has large oscillations when the scaled microwave field is varied, as a consequence of secondary resonances occurring in the primary island where the wave packet is localized. The chaotic ionization rate increases very rapidly at low F_0, as a consequence of the destruction of barriers slowing down the chaotic diffusion towards ionization, and further saturates at a rather constant value when chaotic dynamics is reached.

beginning of Sec. IV C, all our results are obtained either in the perturbative regime $\sigma,\gamma\ll\Delta$ or close to it, and the mean spacing Δ is just a scaling parameter. A rough estimate of Δ is obtained assuming that only states with similar principal quantum number, let us say differing by less than a factor 2, are efficiently coupled. Experimental results on hydrogen atoms in a linearly polarized microwave field [45] suggest that the physics of ionization is entirely dominated by states with principal quantum number less than $2n_0$ (when the experimental cutoff is changed from infinity to $2n_0$, no important change is observed). At low microwave field, the number of efficiently coupled states is smaller, but this is not the regime of chaotic diffusion we are interested in. Chaotic motion requires overlap between classical resonance islands, i.e., efficient coupling between states of largely different principal quantum numbers. This gives the following approximate mean level spacing, used later in this paper:

$$\Delta\approx\frac{1}{n_0^4}. \tag{34}$$

C. Tunneling and chaotic ionization rates

Figure 5 shows the typical width and shift for the nonspreading wave packet of the hydrogen atom in a circularly polarized microwave field at frequency $\omega=1/(40)^3$, as a function of the scaled electric field $F_0=F(40)^4$. Each point in this curve results from the numerical diagonalization of several hundred matrices, each of typical size several tens of thousands, for neighboring values of the microwave field strength and frequency. The statistical model described above makes it possible to separate the intrinsic huge fluctuations of the ionization rate and extract values of the various couplings. This is very clear in Fig. 5, where both the typical width and the typical shift are relatively smooth functions of the field strength, with short-range fluctuations smaller than a factor 2, whereas the raw shift and width display fluctuations over at least three orders of magnitude; compare Fig. 5 with Fig. 1.

In Fig. 5 one can easily check that the typical width is always smaller than the typical shift by at least one order of magnitude. As the ratio of the two is γ/Δ [see Eq. (33)], this implies that inequality (17) is verified. Also, the typical shift is smaller than the mean level spacing (represented by the dashed line), which, using Eq. (33), shows that inequality (16) is also verified. Altogether, this proves that our data are effectively obtained in the perturbative regime.

The third observation in Fig. 5 is that neither the typical width nor the typical shift is a monotonical increasing function of the microwave field strength, but displays various bumps. These bumps are obviously strongly correlated, which indicates that they are due to variations of the tunneling rate σ rather than variations of γ. Indeed, in Fig. 6 we plot the dimensionless parameters σ/Δ and γ/Δ deduced

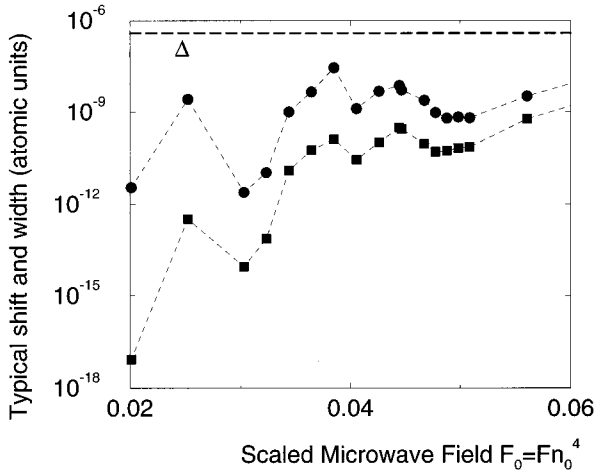

FIG. 7. Plots of the typical shift and width of the nonspreading wave packet, as in Fig. 5, for a hydrogen atom in a linearly polarized microwave field, around $n_0=40$. Again, the typical values of the energy shift (circles) and width (squares) globally increase with the microwave field strength, with bumps that are obviously correlated. The long-dashed line represents the mean energy spacing Δ between chaotic levels (all quantities are plotted in atomic units). The typical width is smaller than the typical shift, itself smaller than Δ, which proves that the data are obtained in the perturbative regime where chaos-assisted tunneling is only a small perturbation.

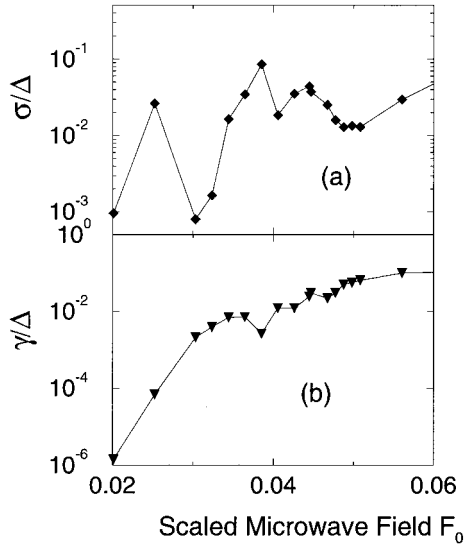

FIG. 8. Same as Fig. 6, but for a hydrogen atom in a linearly polarized microwave. Again, the bumps in (a) σ/Δ are related to the secondary resonances in the system, while (b) γ/Δ is more or less constant as soon as the chaotic regime is reached.

from the typical shift and width. It confirms that the tunneling rate σ/Δ is a slowly increasing function of the field strength with various structures. The bumps occur precisely at values of the field strength where there is a resonance between the eigenfrequencies ω_+ and ω_- [Eq. (8)] of the motion in the vicinity of the stable fixed point supporting the nonspreading wave packet. This has been analyzed in Ref. [40], where it is shown that the bump around $F_0=0.023$ corresponds to the 1:4 resonance and the bump just below $F_0=0.04$ to the 1:3 resonance. In the vicinity of such a resonance, the classical dynamics is strongly perturbed and some secondary resonant tori and islands appear. The bumps in Fig. 6 are just quantum manifestations of an increased transport rate induced by these classical resonances. Not surprisingly, γ/Δ, which represents the ionization rate of states surrounding the resonance island, is practically not affected by these resonances (only small residual oscillations are visible around $F_0=0.04$). On the other hand, it increases very fast up to scaled field $F_0\approx 0.04$, where it saturates to a roughly constant value. This has a simple semiclassical explanation. Below $F_0\approx 0.04$, chaos is not established around the principal resonance island and there still exist some regular tori further in phase space that strongly slow down the classical chaotic diffusion. Above 0.04, only the principal resonance island survives and the chaotic ionization rate is quite large (γ/Δ is of the order of 0.1) and only slowly increases with the field strength.

Strictly similar observations can be made for the hydrogen atom exposed to a linearly polarized microwave field, which proves that they are not specific to one system under study, but rather general properties of chaos-assisted tunneling followed by chaotic diffusion. Figure 7 displays the typical width and typical shift of the nonspreading wave packet for $n_0=40$, as a function of the scaled microwave field $F_0=Fn_0^4$. Again, these data are obtained in the perturbative regime [see Eqs. (16) and (17)] and display obviously correlated bumps. The dimensionless tunneling rate σ/Δ and chaotic ionization rate γ/Δ, shown in Fig. 8, indicate that the bumps are due to secondary resonances inside the primary resonance island between the external microwave frequency and the internal Kepler motion. A comparison between Figs. 6 and 8 shows that both the tunneling rate and chaotic ionization rate are of the same order of magnitude in linear and circular polarization, with similar changes versus F_0, up to possibly a roughly constant multiplicative factor. This is a confirmation of the experimental observation that very similar ionization threshold frequency dependences are observed in the two cases provided F_0 is appropriately rescaled [46]. As in [46] we observe that larger values of F_0 are necessary in LPMs to result in the behavior similar to that for CPMs.

To make the study complete, we have also studied how the typical width and the typical shift change when the principal quantum number n_0 or, equivalently, the microwave frequency $\omega=1/n_0^3$ is changed. The result is shown in Fig. 9 for the circular polarization, for a fixed scaled microwave field $F_0=0.0426$. In this plot, the classical dynamics of the system is absolutely fixed, the only varying parameter being the effective Planck constant $\hbar_{\text{eff}}=1/n_0$. The striking phenomenon is the fast decrease of both the typical width and typical shift with n_0. In the logarithmic scale of Fig. 9, it appears as a straight line indicating an exponential decrease with n_0. Also, the two quantities decrease along parallel lines, which, according to Eq. (33), indicates that the tunneling rate σ is responsible for this decrease. In Fig. 10 we plotted the dimensionless tunneling rate σ/Δ and chaotic ionization rate γ/Δ as a function of n_0. Note that σ/Δ is plotted using a logarithmic scale and γ/Δ on a linear scale. The exponential decrease is of the form

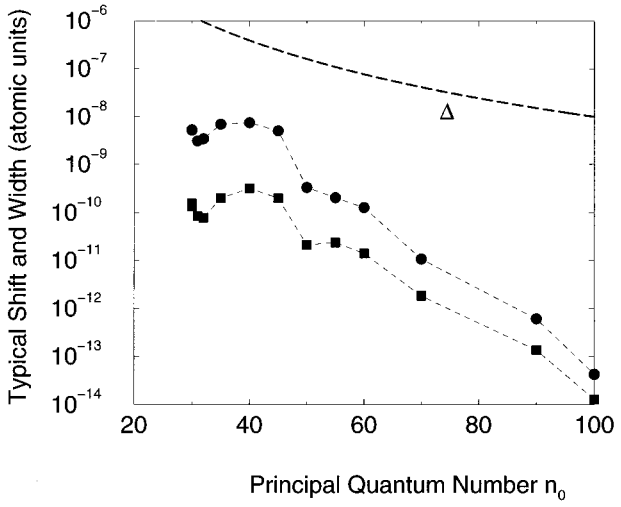

FIG. 9. Same as Fig. 5, but plotted for fixed classical dynamics (fixed $F_0=0.0426$) as a function of the effective principal quantum number $n_0=1/\hbar_{\rm eff}$. Because the primary resonance island has a fixed structure, the bumps visible in Fig. 5 are almost absent. Both the typical shift and typical width decrease exponentially with n_0, a signature of a tunneling process. The long-dashed curve shows the mean energy spacing Δ between chaotic states.

$$\sigma/\Delta \simeq \exp(-n_0 S) = \exp\left(-\frac{S}{\hbar_{\rm eff}}\right), \tag{35}$$

with $S \approx 0.06 \pm 0.01$ (extracted from the plot).

Such a dependence is typical for a tunneling process. S then represents the tunneling action from the stable fixed point where the wave packet sits in the chaotic region surrounding the resonance island. If complex orbits are used, S can be thought of as the imaginary part of the action of a complex tunneling orbit [49,50]. In our realistic system, finding such complex orbits is much more difficult than in the few model systems where this analysis has been done. We have not been able to find the complex path associated with the tunneling process, but our purely quantum results may provide a guide in this search, as they show that the imaginary action has to be of the order of 0.06 for $F_0=0.0426$.

On a linear scale (see Fig. 11) the dimensionless chaotic ionization rate γ/Δ is a slowly increasing function of n_0. A simple classical analysis using the so-called Kepler map [34], which is known to produce relatively good predictions for the ionization threshold of Rydberg states by a microwave field [23,47], predicts a linear dependence versus n_0, while the numerical result seems rather a quadratic function. This discrepancy could be due either to the approximations done to obtain the Kepler map or to the fact that, for high n_0, the statistical model used to extract γ/Δ [see Eqs. (18), (20), (22), and (33)] is no longer valid because several ionization channels are open (see Sec. IV D).

Let us note that to get 800 data points for $n_0=100$ (enough to determine the typical shift and width) requires about 40 h of Cray J98 single processor CPU time. The results presented are, in this sense, quite costly (the size of diagonalized matrices exceeded 200 000 in this case).

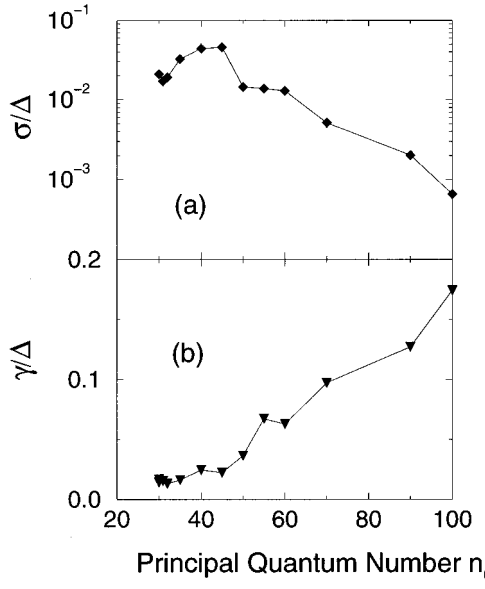

FIG. 10. Same as Fig. 6, but plotted for fixed classical dynamics (fixed $F_0=0.0426$) as a function of the effective principal quantum number $n_0=1/\hbar_{\rm eff}$. (a) The tunneling rate σ/Δ decreases exponentially with n_0 (note the logarithmic scale), which proves that the process involved is actually tunneling. From the rate of the exponential decrease we are able to extract the ''tunneling action'' $S=0.06\pm0.01$. (b) The chaotic ionization rate γ/Δ smoothly and slowly evolves with n_0 (note the linear scale), approximately as n_0^2.

D. Limitations of the model

Although the simple statistical model well describes the fluctuations of the width and shift of the nonspreading wave packet for a range of scaled microwave field ($F_0 \in [0.03,0.08]$ for LPMs and $F_0 \in [0.02,0.06]$ for CPMs, both for n_0 around 40), the region where experiments are usually done, additional difficulties appear for lower and higher field values.

For lower F_0 values, a statistically significant part of the data show very small widths, at the limits of the numerical precision. At the same time, plots of the wave packets similar to those shown in [20] suggest that the states are more extended, extending far from the stable island. The situation then may not correspond to a clear-cut case of the chaos-assisted tunneling process. Our LPM data indicate that in such cases the singularity for small widths is much stronger than $\Gamma^{-1/2}$. Similarly, in the CPM case, we did not present the random matrix fit for $F_0=0.038$, as a significant part of the data is affected there by a strong classical 1:3 resonance [40]. Thus we do not face a clear case of a single localized state but rather two strongly coupled localized states decaying via a chaos-assisted tunneling process. Since such a case is quite rare, we prefer to exclude it from the analysis and not to construct the extension of the random matrix theory. It could not be tested convincingly on a single case anyway.

Most importantly, we could not extend the random model fits to higher F_0 values for a very simple reason. There we observed indications of the opening of other ionization channels [see Eq. (15)]. A typical signature of such a behavior is the disappearance of the singularity $\Gamma^{-1/2}$ in the distribution of the widths. To understand this, note that the typical

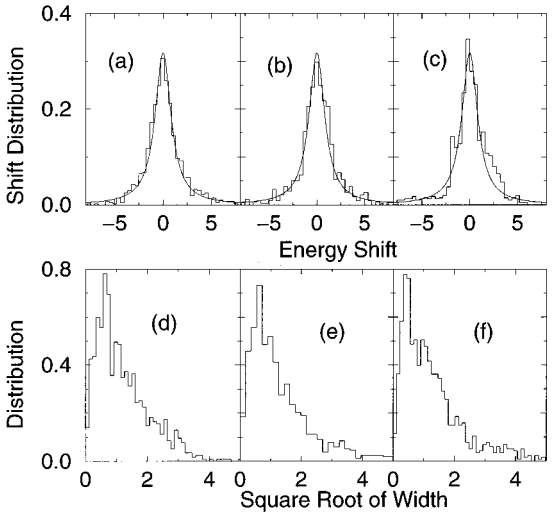

FIG. 11. (a)–(c) Dimensionless shift distribution and (d)–(f) distribution of the square root of the dimensionless width for the nonspreading wave packet of a hydrogen atom in a microwave field. The distributions of the square root of the width deviate from our simple statistical model, which predicts a Cauchy law, because several ionization channels are opened at high field strength or for large n_0. On the contrary, as predicted by the model, the distributions of shifts remain close to Cauchy distributions [solid lines in panels (a)–(c)] and are not sensitive to the number of open channels. (a) and (d) correspond to a circularly polarized microwave field, $n_0=40$, $F_0=0.068$; (b) and (e) correspond to a circularly polarized microwave field, $F_0=0.045$, but $n_0=90$, i.e., for a much smaller average frequency $\omega=1/n_0^3$, which is deeper in the semiclassical regime; and (c) and (f) correspond to a linearly polarized microwave field, $n_0=40$, $F_0=0.076$.

Porter-Thomas distribution behaves, for small widths, as $\Gamma^{M/2-1}$, with M being the number of open channels [41,43]. In the chaos-assisted tunneling process leading to ionization, while the full distribution differs from the Porter-Thomas distribution, as exemplified earlier for the single-channel case, the small width functional behavior is similar in both cases.

The study of the available data reveals that the opening of the second and possibly the third ionization channel appears gradually with the increasing microwave amplitude F_0. Thus the different possible ionization channels are not of equal importance, i.e., they are not equivalent (in the language of the random matrix theory [39]). To build the random matrix model of the process one then needs to introduce additional free parameters describing the strength of the coupling to the additional ionization channels, i.e., various values for the γ_k in Eq. (15). Although such a procedure is quite straightforward, it is clear that fitting these parameters to two data sets (shifts and widths) provides little information and must be ambiguous. Typical distributions of the square root of the width obtained for large microwave amplitudes are presented in Fig. 11 for LPM and CPM wave packets. Note the presence of the hole for small widths.

On the other hand, since in the perturbative limit the level shifts depend only on the real coupling between the localized state and the remaining chaotic subspace [Eqs. (19) and (33)], one can expect that the shifts will be still well described by the Cauchy law (18) independently of the opening of additional ionization channels. Indeed, it is the case as exemplified in Fig. 11 for LPM and CPM wave packets.

Similarly, the opening of additional ionization channels is expected in the semiclassical limit. The limit is realized by decreasing the microwave frequency; then the wave packet is composed of circular states of higher n_0. While the data corresponding to the single-channel decay have been obtained for $n_0=40$ at $F_0=0.0426$, we observed the opening of the second channel for the same F_0 starting at $n_0=60$. Figure 11(e) presents the histogram of the square root of the width for $n_0=90$ and shows the existence of at least two open channels. Again the corresponding shift distribution is not affected and is well described by the Cauchy distribution [Fig. 11(b)].

V. PHYSICAL INTERPRETATION AND CONCLUSIONS

We have presented a statistical theory of ionization catalyzed by chaos-assisted tunneling. The corresponding physical picture is built of a single state, localized on a stable island, and coupled (quantum mechanically, due to a finite value of $\hbar$) to the surrounding chaotic sea. Once the tunneling into the sea takes place, the diffusive chaotic excitation leads finally to ionization.

A random matrix theory model allows us to determine analytically the distribution of the energy shifts (induced by the interaction with the chaotic sea) of the localized state, as well as the distribution of its widths (ionization rates), in the perturbative limit. Nonperturbative corrections may also be understood and estimated. We concentrated on the simplest case of single-channel ionization: The model then is characterized by few parameters only. In that case, the distributions of both shifts and widths have long algebraic tails explaining the large scale fluctuations of both quantities. These fluctuations are a characteristic feature of chaos-assisted tunneling processes. Fluctuations (and universal properties of fluctuations) are well established properties of chaotic systems. In the ionization brought about by chaos-assisted tunneling, the combination of a weak tunneling process with chaotic coupling to the continuum increases dramatically the range of the fluctuations, by extending the distribution considerably towards extremely small widths, i.e., metastable states.

The developed theory has been confronted with numerical data obtained for the shifts and widths of nonspreading wave packets (states localized on a stable 1:1 resonance island between the Kepler frequency of a Rydberg electron and the frequency of an externally applied microwave field of either linear or circular polarization), a system accessible to present experiments. The numerical data have been obtained for simplified models of the atom: a one-dimensional atom in LPMs and a two-dimensional atom in CPMs. This allowed us to study the frequency range well in the experimental region: The important atomic states building the wave packet correspond to the principal quantum numbers used in the experiments. The principal reason for the simplification is that fully three-dimensional numerical calculations, although possible for a single set of parameters as exemplified by us before [24], are still prohibitive for present day computers. More importantly, however, the statistical properties of nonspreading wave packet states are not affected by the reduced di-

mensionality of the atom as tested by us for the three-dimensional CPM case.

It turns out that the statistical theory developed describes very well the numerical data in the range of the single channel decay, which makes us confident that it contains the essential ingredients of the physical process. The quality of the fits allows one to extract order from chaos, that is, to extract from strongly fluctuating quantities (see Fig. 1) the physical parameters describing the coupling of the nonspreading wave packet to the chaotic states (tunneling rate) and the ionization rate of chaotic states. These parameters exhibit reasonably smooth behavior. For example, we have shown that secondary classical resonances inside the regular island increase the tunneling rate. As an unambiguous signature of a tunneling process we also could demonstrate the exponential decrease of the tunneling rate with the principal quantum number.

Let us emphasize the importance of the fluctuations of the ionization rate (width) of nonspreading wave packets in the hydrogen atom. In a real experiment, it is likely that the atoms will experience various values of the microwave field strength, either because of spatial inhomogeneities or because they are prepared by a slow increase of the microwave strength as explained in [48], and more or less average the short range fluctuations of the ionization rate. In the total, the residual ionization of the atom will be given by the average ionization rate, a quantity that is dominated by the fluctuations towards large ionization rates and can be significantly larger than the typical ionization rate. For example, for the data in Fig. 1 discussed in this paper, the average ionization rate is about 6.4 times larger than the typical ionization rate. In the limit of the perturbative regime, the ratio of the two even diverges. This is an example of physical processes as Lévy flights where the physics of a fluctuating system is dominated by rare events.

From a practical point of view, the present study also tells us that the lifetimes of the nonspreading wave packets either in CPMs or in LPMs are rather long. Indeed, for $n_0=60$ and $F_0=0.0426$ (these values are representative of what could be used in a real experiment, with microwave frequency around 30 GHz and microwave field amplitude of the order of 10 V/cm) the typical lifetime of the nonspreading wave packet in CPMs, due to ionization catalyzed by chaos-assisted tunneling, is of the order of several microseconds, that is about 100 000 Kepler periods. However, fluctuations by one or two orders of magnitude are expected around this typical value. Even the longest lifetimes should be shorter than the natural lifetime, due to spontaneous emission, of the order of a fraction of a second. At higher $n_0 \simeq 100$, the typical ionization lifetime is of the order of several milliseconds, i.e., 10×10^6 Kepler periods, but still shorter than the lifetime induced by spontaneous emission [28]. Hence, for practical experiments in CPMs, spontaneous emission should not be a problem. In LPMs, spontaneous emission is a slightly stronger effect, but largely dominated by chaos-assisted tunneling ionization for $n_0 \leqslant 100$ [27].

Finally, the physical situation and the model described here are not restricted to atomic nonspreading wave packets. It should describe physical systems where a given state is weakly coupled to a dense family of completely different other states that can decay on a rather long time scale. Then the effective decay rate of the initial state, induced by the coupling with the family of decaying states, should present huge fluctuations. An example is given in nuclear physics by the so-called superdeformed nuclei [51] where the ground state of a superdeformed nucleus can only decay by coupling to highly excited (hence chaotic) states of the nondeformed nucleus. Our model then predicts the distribution of lifetimes of superdeformed nuclei.

ACKNOWLEDGMENTS

CPU time on a Cray C98 computer has been provided by IDRIS and RZG. Laboratoire Kastler Brossel de l'Université Pierre et Marie Curie et de l'Ecole Normale Supérieure is unité Associée 18 du CNRS. J.Z. acknowledges support of KBN under Project No. 2P03B 03810. The additional support under the bilateral collaboration scheme (J.Z. and D.D.) of the French Embassy in Poland, Project No. 76209, and the Program International de Coopération Scientifique (CNRS) Project No. 408, is appreciated.

APPENDIX: DERIVATION OF SHIFT AND WIDTH DISTRIBUTIONS

We derive here the shift and width distributions for the random matrix model described in Sec. III. Starting from the Hamiltonian (11) we want to compute the complex eigenvalue close to zero. The real part will be the desired shift and twice the imaginary part taken with the minus sign the desired width.

We are interested in the case where the real coupling σ and the imaginary coupling γ are sufficiently small for the localized state not to be strongly mixed with the chaotic states. If this condition is not fulfilled, the localized state cannot be assigned to a given eigenstate of the full $\mathcal{H}$ matrix and the shift and width are ill-defined quantities. In the following, we thus consider the perturbative limit where both σ and γ are much smaller than Δ. Typically, the localized state is then weakly coupled to the chaotic sea, itself weakly coupled to the continuum. It may happen that the localized state is accidentally almost degenerate with a chaotic eigenstate of H_0, bringing back the problem of assigning the strongly mixed state. However, this is a rare event, which, as it is shown below, affects the tails of the distributions only. In the generic case, the couplings are weak and the energy shift and the width can be calculated perturbatively.

There are two small parameters for the perturbative analysis, namely, σ/Δ and γ/Δ. At first order in these small parameters, there is no effect on the energy of the localized state (no diagonal element). On the other hand, the localized state is contaminated at first order in σ/Δ by the chaotic states. The perturbed eigenstate $|\widetilde{0}\rangle$ can be written as

$$|\widetilde{0}\rangle = |0\rangle + \sigma \frac{1}{H_0}|V\rangle, \tag{A1}$$

where $|0\rangle$ denotes the unperturbed localized state and $|V\rangle$ is the N-component vector describing the coupling of the localized state to the chaotic states. It can be also expanded on the eigenstates $|\phi_i\rangle$ of H_0 with eigenvalues E_i as

$$|\widetilde{0}\rangle = |0\rangle + \sigma \sum_{i=1,N} \frac{\langle \phi_i|V\rangle |\phi_i\rangle}{E_i}. \tag{A2}$$

This admixture in the eigenstate results in a (real) energy shift at second order, i.e., proportional to σ^2, given by

$$s = -\sigma^2 \left\langle V \left| \frac{1}{H_0} \right| V \right\rangle = -\sigma^2 \sum_{i=1}^{N} \frac{|\langle \phi_i|V\rangle|^2}{E_i}. \tag{A3}$$

Also, as the imaginary coupling $-i\mathcal{W}$ [Eqs. (11) and (14)] has nonzero diagonal elements, this implies a nonzero imaginary part of the energy at order $\sigma^2\gamma$ or, more precisely, a width given by

$$w = \gamma\sigma^2 \left| \left\langle W \left| \frac{1}{H_0} \right| V \right\rangle \right|^2 = \gamma\sigma^2 \left| \sum_{i=1}^{N} \frac{\langle W|\phi_i\rangle \langle \phi_i|V\rangle}{E_i} \right|^2. \tag{A4}$$

Since w appears as the square of a simpler quantity x, i.e.,

$$w = x^2, \tag{A5}$$

with x given by,

$$x = \sqrt{\gamma}\sigma \left\langle W \left| \frac{1}{H_0} \right| V \right\rangle = \sqrt{\gamma}\sigma \sum_{i=1,N} \frac{\langle W|\phi_i\rangle\langle \phi_i|V\rangle}{E_i}, \tag{A6}$$

we will consider in the following the statistical distribution of x rather than w.

To obtain the statistical distributions within our random matrix model, one has to average over the random ensemble, i.e., over the various Gaussian random variables: the N components of $|V\rangle$, the N components of $|W\rangle$, and the $N(N+1)/2$ independent matrix elements of H_0. Because of the orthogonal invariance of H_0, the averaging over $|V\rangle$ and $|W\rangle$ is straightforward. Thus the distribution of shift is essentially the distribution of diagonal elements of $1/H_0$, while the distribution of x (square root of the width) is essentially the distribution of matrix element of $1/H_0$ between two statistically independent vectors.

Since we are interested in the situation where a large number of chaotic states are coupled to the localized state, we will take the limit $N\to\infty$, keeping the mean level spacing equal to a constant Δ and keeping γ and σ fixed, such that the average coupling between a chaotic state and the localized state is independent of N. Then, in the sums in Eqs. (A3) and (A6), there are more and more terms that contribute as N is increased, but corresponding to larger and larger energy denominators $1/E_i$ so that the total sum has a well-defined limit as $N\to\infty$. Yet, in this limit, the scalar product $\langle W|V\rangle = \Sigma \langle W|\phi_i\rangle\langle\phi_i|V\rangle$ appears as the sum of the product of independent Gaussian variables, which typically averages to a small quantity. In other words, in the $N\to\infty$ limit, $|V\rangle$ and $|W\rangle$ appear as independent orthogonal vectors, so that the distribution of x values is essentially the distribution of nondiagonal elements of $1/H_0$. Corrections due to nonexact orthogonality will modify the distribution at order $1/N$ only.

The calculation of the sums in Eqs. (A3) and (A6) is not completely straightforward because the various energies in the denominators are *correlated* if H_0 is a GOE random matrix. Before studying this case, let us consider the simpler case where the spectrum of H_0 is a set of *uncorrelated* eigenvalues, i.e., a Poisson spectrum. Then all quantities in the numerators are uncorrelated random Gaussian variables and denominators are uncorrelated energies with mean density $1/\Delta$. In this case, the calculation can be done exactly as shown in Refs. [15,52] and the distribution is a Cauchy distribution whose half-width is proportional to the average absolute value of the numerator, that is,

$$P_{\text{Poisson}}(s) = \frac{1}{\pi} \frac{s_0}{s_0^2 + s^2}, \tag{A7}$$

with

$$s_0 = \pi \frac{\sigma^2 \overline{|\langle \phi_i|V\rangle|^2}}{\Delta}, \tag{A8}$$

where the overbar denotes the average value over the random matrix ensemble. Here it is simply the variance of the components of $|V\rangle$, which is 1 in our model (see Sec. III). Hence

$$s_0 = \frac{\pi\sigma^2}{\Delta}. \tag{A9}$$

Similarly, one gets

$$P_{\text{Poisson}}(x) = \frac{1}{\pi} \frac{x_0}{x_0^2 + x^2}, \tag{A10}$$

with

$$x_0 = \pi \frac{\sigma\sqrt{\gamma}\,\overline{|\langle W|\phi_i\rangle\langle\phi_i|V\rangle|}}{\Delta}. \tag{A11}$$

The average over the random ensemble (Gaussian integral) gives a $2/\pi$ factor, resulting in

$$x_0 = \frac{2\sigma\sqrt{\gamma}}{\Delta}. \tag{A12}$$

For the width itself, we obtain the distribution given in Sec. III [Eq. (20)].

We now turn to the random matrix case, where H_0 is a standard real symmetric random matrix belonging to the GOE. In Ref. [53], Brouwer introduced a slightly different class of random matrices, namely, the Lorentzian orthogonal ensemble (LOE), which has the Lorentzian probability distribution

$$P(H) = \left(\frac{\lambda^2}{\pi}\right)^{N(N+1)/4} \prod_{i=1,N} \frac{\Gamma(i)}{\Gamma(i/2)} \det[(\lambda^2 + H^2)^{-(N+1)/2}], \tag{A13}$$

where λ is a parameter describing the width of the distribution.

As shown in Ref. [53], although the LOE has different global statistical properties (e.g., density of states) from the GOE, it has locally the same joint probability distribution function of the eigenvalues and consequently the same spacing distribution, the same short range correlation functions, etc. The mean level spacing close to the center of the spectrum (energy equal to zero) is

$$\Delta = \frac{\lambda \pi}{N}. \tag{A14}$$

Hence, to calculate the shift and the width distribution, we can replace H_0 by a random matrix of the LOE. The LOE has the nice property [53] that if H_0 is distributed according to LOE, then $1/H_0$ is also distributed according to LOE with width $1/\lambda$. Morevoer, if H_0 is distributed according to the LOE, then every submatrix of H_0 is also distributed according to LOE, with the same width [53]. The price to pay for such nice properties is that one loses the statistical independence of the various matrix elements valid for the GOE, i.e., $P(H)$ cannot be factorized as a product of distributions of elementary matrix elements. However, this is not a problem for the quantities we are interested in. The distribution of shifts is obtained straightforwardly, as it is a diagonal element of $1/H_0$, and hence a 1×1 submatrix of $1/H_0$, which, from the two properties just described, is given by Eq. (A13) for $N=1$ and $\lambda = \pi/N\Delta$. The result is exactly equal to the Poisson result, i.e., the Cauchy (or Lorentzian) distribution of Eq. (A9).

For the width, the situation is slightly more complicated as we need to know the distribution of a nondiagonal element of $1/H_0$. The same trick works, but we have now to extract for the LOE matrix $1/H_0$ a 2×2 submatrix and consider the distribution of nondiagonal elements, that is, average over the two diagonal elements

$$P(H_{12}) = \int \int P(H) dH_{11} dH_{22}, \tag{A15}$$

where $P(H)$ is given by Eq. (A13) for $N=2$ and $\lambda = \pi/N\Delta$. The integral over diagonal elements is trivial. The result is the following distribution for the square root of the width:

$$P_{\mathrm{GOE}}(x) = \frac{2x_0'}{\pi^2(x_0'^2+x^2)}\left[1+\frac{\mathrm{arcsinh}(x/x_0')x_0'^2}{x\sqrt{x_0'^2+x^2}}\right], \tag{A16}$$

with

$$x_0' = \frac{\pi\sigma\sqrt{\gamma}}{\Delta}. \tag{A17}$$

For the width itself, we obtain the distribution given in Sec. III [Eq. (22)].

The GOE distribution (A16) has the same behavior as the Cauchy distribution obtained for the Poisson ensemble (A10), which is a constant value near $x=0$ followed by a $1/x^2$ decrease at large distance. In fact, the two distributions are very similar with slightly different widths and are almost impossible to distinguish by eye.

The distributions obtained in the various cases agree exactly with numerically calculated distributions from a large number of realizations of the Poisson and GOE random ensembles. Note that the distributions obtained here have long tails with an algebraic decay as s (or x) tends to infinity. This is unusual for quantities that are sums of statistically uncorrelated individual terms and, as a consequence of the central limit theorem, have usually Gaussian distributions. The reason is that the central limit theorem cannot be used here because the variance of each individual term in infinite; see Refs. [15,52]. The latter property is due to the $1/E_i$ dependence, which decays only slowly for large E_i.

On a double-logarithmic scale (see Fig. 2) the distribution of shifts shows two different regimes: constant near the origin and an asymptotic $1/s^2$ behavior for large shifts. The crossover between the two regimes is for $s=s_0$; the latter value [Eq. (A9)] corresponds to the typical shift due to a chaotic level lying at a distance Δ from the localized state, i.e., to the typical shift due to the nearest state. Hence large energy shifts $s \gg s_0$ are due to situations where one chaotic level is much closer in energy than Δ. In such a case, one term is dominant in the sum (A3) and a two-level approximation can be used, which produces the correct $1/s^2$ behavior. On the other hand, the ''constant'' regime $s \ll s_0$ corresponds to situations where the various terms in Eq. (A3) interfere destructively, giving a total sum typically smaller than the largest individual terms: This is an intrisically ''multilevel'' situation where quantum destructive interferences play an important role. Exactly the same thing takes place for the distribution of widths. The largest widths in the $w^{-3/2}$ regime are obtained when a single level dominates the sum (A6) while the $w^{-1/2}$ regime correspond to the multilevel situation.

Finally, let us discuss what happens when the perturbative approach breaks down. This takes place when one chaotic level is very close to the localized level, closer than their average coupling σ. There the strong mixing between states invalidate the expressions for the shift [Eq. (A3)] and the width [Eq. (A6)]. The actual shift and width do not diverge, in contrast to the perturbative expressions. This means that the actual distribution cannot have an algebraic tail towards infinity, but should show a cutoff when perturbation theory breaks down. As explained above, this takes place for one of the E_i of the order of σ, corresponding to

$$s_{\mathrm{cutoff}} \simeq \sigma, \tag{A18}$$

$$w_{\mathrm{cutoff}} \simeq \gamma, \tag{A19}$$

in agreement with our numerical observations.

[1] A. M. Ozorio de Almeida, *Hamiltonian Systems: Chaos and Quantization* (Cambridge University Press, Cambridge, 1988); M. C. Gutzwiller, *Chaos in Classical and Quantum Mechanics* (Springer-Verlag, New York, 1990); L. E. Reichl, *The Transition to Chaos: In Conservative Classical Systems: Quantum Manifestations* (Springer-Verlag, New York 1992).

[2] F. Haake, in *Quantum Signatures of Chaos*, edited by H. Haken, Springer Series in Synergetics Vol. 54 (Springer-Verlag, Berlin, 1991).

[3] Sh.-J. Chang and K.-J. Shi, Phys. Rev. A **34**, 7 (1986); R. V.

Jensen, M. M. Sanders, M. Saraceno, and B. Sundaram, Phys. Rev. Lett. **63**, 2771 (1989).
[4] M. Holthaus, Chaos Solitons Fractals **5**, 1143 (1995), and references therein.
[5] E. Heller, Phys. Rev. Lett. **53**, 1515 (1984).
[6] I. C. Percival, J. Phys. B **6**, L229 (1973).
[7] V. P. Maslov and M. V. Fedoriuk, *Semiclassical Approximation in Quantum Mechanics* (Reidel, Dordrecht, 1981).
[8] A. J. Lichtenberg and M. A. Liberman, *Regular and Chaotic Dynamics* (Springer-Verlag, New York, 1992).
[9] W. A. Lin and L. E. Ballentine, Phys. Rev. Lett. **65**, 2927 (1990); Phys. Rev. A **45**, 3637 (1992).
[10] F. Grossmann, T. Dittrich, P. Jung, and P. Hänggi, Phys. Rev. Lett. **67**, 516 (1991); Z. Phys. B **84**, 315 (1991); J. Stat. Phys. **70**, 229 (1993).
[11] J. Plata and J. M. Gomez Llorente, J. Phys. A **25**, L303 (1992).
[12] O. Bohigas, S. Tomsovic, and D. Ullmo, Phys. Rep. **223**, 43 (1993).
[13] O. Bohigas, D. Boosé, R. Egydio de Carvalho, and V. Marvulle, Nucl. Phys. A **560**, 197 (1993).
[14] S. Tomsovic and D. Ullmo, Phys. Rev. E **50**, 145 (1994).
[15] F. Leyvraz and D. Ullmo, J. Phys. A **29**, 2529 (1996).
[16] P. Gerwinski and P. Šeba, Phys. Rev. E **50**, 3615 (1994).
[17] A. Buchleitner, thèse de doctorat, Université Pierre et Marie Curie, 1993 (unpublished); D. Delande and A. Buchleitner, Adv. At., Mol., Opt. Phys. **35**, 85 (1994); A. Buchleitner and D. Delande, Phys. Rev. Lett. **75**, 1487 (1995); Chaos Solitons Fractals **5**, 1125 (1995).
[18] I. Bialynicki-Birula, Maciej Kaliński, and J. H. Eberly, Phys. Rev. Lett. **73**, 1777 (1994).
[19] J. H. Shirley, Phys. Rev. **138**, B979 (1965).
[20] D. Delande, J. Zakrzewski, and A. Buchleitner, Europhys. Lett. **32**, 107 (1995).
[21] F. V. Bunkin and A. Prokhorov, Zh. Eksp. Teor. Fiz. **46**, 1090 (1964) [Sov. Phys. JETP **19**, 739 (1964)].
[22] T. P. Grozdanov, M. J. Raković, and E. A. Solov'ev, J. Phys. B **25**, 4455 (1992).
[23] J. Zakrzewski, R. Gębarowski, and D. Delande, Phys. Rev. A **54**, 691 (1996).
[24] J. Zakrzewski, D. Delande, and A. Buchleitner, Phys. Rev. Lett. **75**, 4015 (1995).
[25] See, e.g., D. Delande, in *Chaos and Quantum Physics*, 1989 Les Houches Lectures, Session LII, edited by M.-J. Giannoni, A. Voros, and J. Zinn-Justin (North-Holland, Amsterdam, 1991), p. 665.
[26] W. P. Reinhardt, Annu. Rev. Phys. Chem. **33**, 323 (1982); Y. K. Ho, Phys. Rep. **99**, 1 (1983).
[27] K. Hornberger and A. Buchleitner (unpublished).
[28] Z. Bialynicka-Birula and I. Bialynicki-Birula, Phys. Rev. A **56**, 3623 (1997).
[29] D. Delande, A. Bommier, and J.-C. Gay, Phys. Rev. Lett. **66**, 141 (1991).
[30] C. Cohen-Tannoudji, in *New Trends in Atomic Physics*, Proceedings of the Les Houches Summer School of Theoretical Physics, Session XXXVIII, edited by G. Grynberg and R. Stora (North-Holland, Amsterdam, 1984).
[31] G. P. Berman and G. M. Zaslavsky, Phys. Lett. **61A**, 295 (1977).
[32] L. Sirko and P. M. Koch, Appl. Phys. B: Lasers Opt. **60**, 195 (1995).
[33] J. Henkel and M. Holthaus, Phys. Rev. A **45**, 1978 (1992).
[34] G. Casati, I. Guarneri, and D. Shepelyansky, IEEE J. Quantum Electron. **24**, 1420 (1988).
[35] A. Bucheitner and D. Delande, Phys. Rev. A **55**, R1585 (1997).
[36] n_0 is defined from the microwave frequency through Eq. (3) and is not necessarily an integer. Therefore, we identify the wave packet by its large overlap with the hydrogenic state $|n\rangle$ with n the closest integer to n_0.
[37] S. Washburn and R. Webb, Adv. Phys. **35**, 375 (1986); D. Mailly and M. Sanquer, J. Phys. I **2**, 357 (1992); P. A. Lee and A. D. Stone, Phys. Rev. Lett. **55**, 1622 (1985).
[38] O. Bohigas, in *Chaos and Quantum Physics* (Ref. [25]), p. 87.
[39] F. Haake, F. Izrailev, N. Lehmann, D. Saher, and H.-J. Sommers, Z. Phys. B **88**, 359 (1992).
[40] J. Zakrzewski, A. Buchleitner, and D. Delande, Z. Phys. B **103**, 115 (1997).
[41] T. A. Brody *et al.*, Rev. Mod. Phys. **53**, 385 (1981), and references therein.
[42] B. Grémaud, D. Delande, and J. C. Gay, Phys. Rev. Lett. **70**, 1615 (1993).
[43] K. Dupret, J. Zakrzewski, and D. Delande, Europhys. Lett. **31**, 251 (1995).
[44] See, e.g., M. F. Shlesinger, G. M. Zaslavsky, and J. Klafter, Nature (London) **263**, 31 (1993); G. Zumofen and J. Klafter, Phys. Rev. E **47**, 851 (1993); J. B. Bouchaud and A. Georges, Phys. Rep. **195**, 136 (1990).
[45] P. M. Koch and K. A. H. van Leeuwen, Phys. Rep. **255**, 289 (1995).
[46] M. R. W. Bellermann, P. M. Koch, D. R. Mariani, and D. Richards, Phys. Rev. Lett. **76**, 892 (1996).
[47] A. Buchleitner and D. Delande, Phys. Rev. Lett. **70**, 33 (1993).
[48] J. Zakrzewski and D. Delande, J. Phys. B **30**, L87 (1997).
[49] S. Creagh and N. Whelan, Phys. Rev. Lett. **77**, 4975 (1996).
[50] P. Leboeuf and A. Mouchet, Phys. Rev. Lett. **73**, 1360 (1994).
[51] T. Bengtsson, I. Ragnarsson, and S. Åberg, Phys. Lett. B **208**, 39 (1988).
[52] P. A. Mello, in 1994 Les Houches Lectures, Session LXI, Mesoscopic Quantum Physics, edited by E. Akkermans, G. Montambaux, J. L. Pichard, and J. Zinn-Justin (North-Holland, Amsterdam, 1995), p. 435.
[53] P. W. Brouwer, Phys. Rev. B **51**, 16 878 (1995).